

# Delving Deep into Rectifiers: Surpassing Human-Level Performance on ImageNet Classification

Kaiming He    Xiangyu Zhang    Shaoqing Ren    Jian Sun  
 Microsoft Research

## Abstract

*Rectified activation units (rectifiers) are essential for state-of-the-art neural networks. In this work, we study rectifier neural networks for image classification from two aspects. First, we propose a Parametric Rectified Linear Unit (PReLU) that generalizes the traditional rectified unit. PReLU improves model fitting with nearly zero extra computational cost and little overfitting risk. Second, we derive a robust initialization method that particularly considers the rectifier nonlinearities. This method enables us to train extremely deep rectified models directly from scratch and to investigate deeper or wider network architectures. Based on the learnable activation and advanced initialization, we achieve 4.94% top-5 test error on the ImageNet 2012 classification dataset. This is a 26% relative improvement over the ILSVRC 2014 winner (GoogLeNet, 6.66% [33]). To our knowledge, our result is the first<sup>1</sup> to surpass the reported human-level performance (5.1%, [26]) on this dataset.*

## 1. Introduction

Convolutional neural networks (CNNs) [19, 18] have demonstrated recognition accuracy better than or comparable to humans in several visual recognition tasks, including recognizing traffic signs [3], faces [34, 32], and handwritten digits [3, 36]. In this work, we present a result that surpasses the human-level performance reported by [26] on a more generic and challenging recognition task - the classification task in the 1000-class ImageNet dataset [26].

In the last few years, we have witnessed tremendous improvements in recognition performance, mainly due to advances in two technical directions: building more powerful models, and designing effective strategies against overfitting. On one hand, neural networks are becoming more capable of fitting training data, because of increased complexity (*e.g.*, increased depth [29, 33], enlarged width [37, 28], and the use of smaller strides [37, 28, 2, 29]), new non-linear activations [24, 23, 38, 22, 31, 10], and sophisticated layer designs [33, 12]. On the other hand, better generalization is achieved by effective regularization

techniques [13, 30, 10, 36], aggressive data augmentation [18, 14, 29, 33], and large-scale data [4, 26].

Among these advances, the rectifier neuron [24, 9, 23, 38], *e.g.*, Rectified Linear Unit (ReLU), is one of several keys to the recent success of deep networks [18]. It expedites convergence of the training procedure [18] and leads to better solutions [24, 9, 23, 38] than conventional sigmoid-like units. Despite the prevalence of rectifier networks, recent improvements of models [37, 28, 12, 29, 33] and theoretical guidelines for training them [8, 27] have rarely focused on the properties of the rectifiers.

Unlike traditional sigmoid-like units, *ReLU is not a symmetric function*. As a consequence, the mean response of ReLU is always no smaller than zero; besides, even assuming the inputs/weights are subject to symmetric distributions, the distributions of responses can still be asymmetric because of the behavior of ReLU. These properties of ReLU influence the theoretical analysis of convergence and empirical performance, as we will demonstrate.

In this paper, we investigate neural networks from two aspects particularly driven by the rectifier properties. First, we propose a new extension of ReLU, which we call *Parametric Rectified Linear Unit* (PReLU). This activation function adaptively learns the parameters of the rectifiers, and improves accuracy at negligible extra computational cost. Second, we study the difficulty of training rectified models that are very deep. By explicitly modeling the non-linearity of rectifiers (ReLU/PReLU), we derive a theoretically sound initialization method, which helps with convergence of very deep models (*e.g.*, with 30 weight layers) *trained directly from scratch*. This gives us more flexibility to explore more powerful network architectures.

On the 1000-class ImageNet 2012 dataset, our network leads to a single-model result of 5.71% top-5 error, which surpasses all multi-model results in ILSVRC 2014. Further, our multi-model result achieves 4.94% top-5 error on the test set, which is a 26% relative improvement over the ILSVRC 2014 winner (GoogLeNet, 6.66% [33]). To the best of our knowledge, our result surpasses for the first time the reported human-level performance (5.1% in [26]) of a dedicated individual labeler on this recognition challenge.

<sup>1</sup>reported in Feb. 2015.

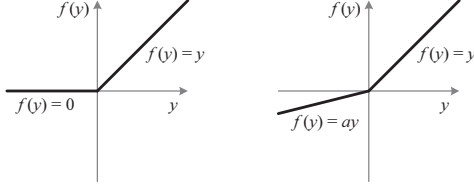


Figure 1. ReLU vs. PReLU. For PReLU, the coefficient of the negative part is not constant and is adaptively learned.

## 2. Approach

In this section, we first present the PReLU activation function (Sec. 2.1). Then we derive our initialization method for deep rectifier networks (Sec. 2.2).

### 2.1. Parametric Rectifiers

We show that replacing the parameter-free ReLU by a learned activation unit improves classification accuracy<sup>2</sup>.

**Definition.** Formally, we define an activation function:

$$f(y_i) = \begin{cases} y_i, & \text{if } y_i > 0 \\ a_i y_i, & \text{if } y_i \leq 0 \end{cases}. \quad (1)$$

Here  $y_i$  is the input of the nonlinear activation  $f$  on the  $i$ th channel, and  $a_i$  is a coefficient controlling the slope of the negative part. The subscript  $i$  in  $a_i$  indicates that we allow the nonlinear activation to vary on different channels. When  $a_i = 0$ , it becomes ReLU; when  $a_i$  is a learnable parameter, we refer to Eqn.(1) as *Parametric ReLU* (PReLU). Figure 1 shows the shapes of ReLU and PReLU. Eqn.(1) is equivalent to  $f(y_i) = \max(0, y_i) + a_i \min(0, y_i)$ .

If  $a_i$  is small and fixed, PReLU becomes Leaky ReLU (LReLU) [23] ( $a_i = 0.01$ ). The motivation of LReLU is to avoid zero gradients. Experiments in [23] show that LReLU has negligible impact on accuracy compared with ReLU. On the contrary, our method adaptively learns the PReLU parameters jointly with the whole model. We hope that end-to-end training will lead to more specialized activations.

PReLU introduces a very small number of extra parameters. The number of extra parameters is equal to the total number of channels, which is negligible when considering the total number of weights. So we expect no extra risk of overfitting. We also consider a channel-shared variant:  $f(y_i) = \max(0, y_i) + a \min(0, y_i)$  where the coefficient is shared by all channels of one layer. This variant only introduces a single extra parameter into each layer.

**Optimization.** PReLU can be trained using backpropagation [19] and optimized simultaneously with other layers. The update formulations of  $\{a_i\}$  are simply derived from

the chain rule. The gradient of  $a_i$  for one layer is:

$$\frac{\partial \mathcal{E}}{\partial a_i} = \sum_{y_i} \frac{\partial \mathcal{E}}{\partial f(y_i)} \frac{\partial f(y_i)}{\partial a_i}, \quad (2)$$

where  $\mathcal{E}$  represents the objective function. The term  $\frac{\partial \mathcal{E}}{\partial f(y_i)}$  is the gradient propagated from the deeper layer. The gradient of the activation is given by:

$$\frac{\partial f(y_i)}{\partial a_i} = \begin{cases} 0, & \text{if } y_i > 0 \\ y_i, & \text{if } y_i \leq 0 \end{cases}. \quad (3)$$

The summation  $\sum_{y_i}$  runs over all positions of the feature map. For the channel-shared variant, the gradient of  $a$  is  $\frac{\partial \mathcal{E}}{\partial a} = \sum_i \sum_{y_i} \frac{\partial \mathcal{E}}{\partial f(y_i)} \frac{\partial f(y_i)}{\partial a}$ , where  $\sum_i$  sums over all channels of the layer. The time complexity due to PReLU is negligible for both forward and backward propagation.

We adopt the momentum method when updating  $a_i$ :

$$\Delta a_i := \mu \Delta a_i + \epsilon \frac{\partial \mathcal{E}}{\partial a_i}. \quad (4)$$

Here  $\mu$  is the momentum and  $\epsilon$  is the learning rate. It is worth noticing that we do not use weight decay ( $l_2$  regularization) when updating  $a_i$ . A weight decay tends to push  $a_i$  to zero, and thus biases PReLU toward ReLU. Even without regularization, the learned coefficients rarely have a magnitude larger than 1 in our experiments. We use  $a_i = 0.25$  as the initialization.

**Comparison Experiments.** The improvement of PReLU over ReLU has been observed on various models. Here we present comparisons on a deep but efficient model with 14 weight layers. The model was studied in [11] (model E of [11]) and its architecture is described in Table 1.

As a baseline, we train this model with ReLU applied in the convolutional (conv) layers and the first two fully-connected (fc) layers. The training implementation follows [11]. The top-1 and top-5 errors are 33.82% and 13.34% on ImageNet 2012, using 10-view testing (Table 2).

Then we train the same architecture from scratch, with all ReLUs replaced by PReLU (Table 2). The top-1 error is reduced to 32.64%. This is a **1.2%** gain over the ReLU baseline. Table 2 also shows that channel-wise/channel-shared PReLU perform comparably. For the channel-shared version, PReLU only introduces 13 extra free parameters compared with the ReLU counterpart. But this small number of free parameters play critical roles as evidenced by the 1.1% gain over the baseline. This implies the importance of adaptively learning the shapes of activation functions.

We also show the result of LReLU with  $a = 0.25$  in Table 2, which is no better than ReLU. In our experiments, we found that choosing the fixed value  $a$  in LReLU very carefully (by cross-validation) can lead to better results than

<sup>2</sup>Concurrently, [1] also investigated learning activations.

layer		learned coefficients	
		channel-shared	channel-wise
conv1	7×7, 64, / <sub>2</sub>	0.681	0.596
pool1	3×3, / <sub>3</sub>		
conv2 <sub>1</sub>	2×2, 128	0.103	0.321
conv2 <sub>2</sub>	2×2, 128	0.099	0.204
conv2 <sub>3</sub>	2×2, 128	0.228	0.294
conv2 <sub>4</sub>	2×2, 128	0.561	0.464
pool2	2×2, / <sub>2</sub>		
conv3 <sub>1</sub>	2×2, 256	0.126	0.196
conv3 <sub>2</sub>	2×2, 256	0.089	0.152
conv3 <sub>3</sub>	2×2, 256	0.124	0.145
conv3 <sub>4</sub>	2×2, 256	0.062	0.124
conv3 <sub>5</sub>	2×2, 256	0.008	0.134
conv3 <sub>6</sub>	2×2, 256	0.210	0.198
spp	{6, 3, 2, 1}		
fc <sub>1</sub>	4096	0.063	0.074
fc <sub>2</sub>	4096	0.031	0.075

Table 1. A small but deep 14-layer model [11]. The filter size and filter number of each layer is listed. The number /*s* indicates the stride *s* that is used. The learned coefficients of PReLU are also shown. For the channel-wise case, the average of  $\{a_i\}$  over the channels is shown for each layer.

	top-1	top-5
ReLU	33.82	13.34
LReLU ( $a = 0.25$ )	33.80	13.56
PReLU, channel-shared	32.71	12.87
PReLU, channel-wise	<b>32.64</b>	<b>12.75</b>

Table 2. Comparisons between ReLU, LReLU, and PReLU on the small model. The error rates are for ImageNet 2012 using 10-view testing. The images are resized so that the shorter side is 256, during both training and testing. Each view is 224×224. All models are trained using 75 epochs.

ReLU, but needs tedious, repeated training. On the contrary, our method adaptively learns this parameter from the data.

Table 1 shows the learned coefficients of PReLUs for each layer. There are two interesting phenomena in Table 1. First, the first conv layer (conv1) has coefficients (0.681 and 0.596) significantly greater than 0. As the filters of conv1 are mostly Gabor-like filters such as edge or texture detectors, the learned results show that both positive and negative responses of the filters are respected. We believe that this is a more economical way of exploiting low-level information, given the limited number of filters. Second, for the channel-wise version, the deeper conv layers in general have smaller coefficients. This implies that the activations gradually become “more nonlinear” at increasing depths. In other words, the learned model tends to keep more information in earlier stages and becomes more discriminative in deeper stages.

**Analysis.** We investigate how PReLU may affect training via computing the Fisher Information Matrix (FIM). If the off-diagonal blocks of FIM are closer to zero, SGD which is a first-order solver becomes closer to natural gradient de-

scent which is second-order and converges faster ([25, 35]). For simplicity, we consider a two-layer MLP with weight matrices *W* and *V*:

$$\mathbf{z} = \mathbf{V}f(\mathbf{W}\mathbf{x}), \quad (5)$$

where *f* is ReLU/PReLU. Following [25, 35], we consider the case where *z* follows a Gaussian distribution  $p \sim \mathcal{N}(\mu, \sigma^2)$  with  $\mu = \mathbf{V}f(\mathbf{W}\mathbf{x})$ . FIM has off-diagonal blocks:

$$-\frac{1}{T} \sum_t \left\langle \frac{\partial}{\partial v_{ij}} \frac{\partial}{\partial v_{i'j'}} \log p \right\rangle = \frac{1}{\sigma_i^2} \delta(i, i') \frac{1}{T} \sum_t f_j(\mathbf{W}\mathbf{x}_t) f_{j'}(\mathbf{W}\mathbf{x}_t), \quad (6)$$

where *i, j, i', j'* are indices of weights,  $\delta(i, i') = 1$  if *i* = *i'* and 0 otherwise, and *t* is the sample index on a batch of a size *T*. The notation  $\langle \cdot \rangle$  is the expectation over the distribution of *z*. Assuming that elements of *y* = *Wx* subject to independent zero-mean Gaussian distributions and the elements in *f* are uncorrelated, we have that in (6) the term  $\frac{1}{T} \sum_t f_j(\mathbf{W}\mathbf{x}_t) f_{j'}(\mathbf{W}\mathbf{x}_t) \approx E[f_j, f_{j'}] = E[f_j]E[f_{j'}]$  where  $E[\cdot]$  is the expectation over samples *x*. As  $E[f] = \frac{1}{2}(E[y|y \geq 0] + aE[y|y < 0])$ , for *a* = 0 (ReLU)  $E[f]$  is greater than 0, and for *a* > 0 (PReLU) it can be closer to 0. So PReLU is able to push these off-diagonal blocks of FIM closer to zero. We note that FIM involves other off-diagonal blocks and it is not realistic for the above assumptions to hold when training evolves, so we evaluated with real data following [25, 35] (see supplementary). We observed that PReLU improves the conditioning, which explains the faster convergence than ReLU as observed in experiments (Figure 4).

In [20, 25, 35] the analysis of FIM was a motivation of *centering* the nonlinear responses of each layer, which eases training of symmetric, sigmoid-like units. But ReLU is not a symmetric function, and has a positive mean. The slope *a* in PReLU is an adaptively learned parameter that can offset the positive mean of ReLU. This hypothesis is justified in Figure 2, in which the mean responses of PReLU is in general smaller than those of ReLU.

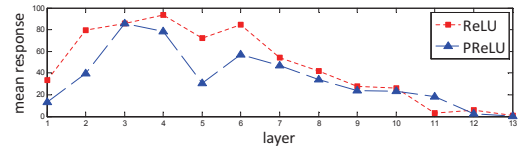


Figure 2. Mean responses of each layer for the trained models in Table 1. PReLU in general has smaller mean responses.

## 2.2. Initialization of Filter Weights for Rectifiers

Rectifier networks are easier to train [9, 18, 38] compared with traditional sigmoid-like activation networks. But a bad initialization can still hamper the learning of a highly non-linear system. In this subsection, we propose a robust initialization method that removes an obstacle of training extremely deep rectifier networks.

Recent deep CNNs are mostly initialized by random weights drawn from Gaussian distributions [18]. With fixed

standard deviations (*e.g.*, 0.01 in [18]), very deep models (*e.g.*, >8 conv layers) have difficulties to converge, as reported by the VGG team [29] and also observed in our experiments. To address this issue, in [29] they pre-train a model with 8 conv layers to initialize deeper models. But this strategy requires more training time, and may also lead to a poorer local optimum. In [33, 21], auxiliary classifiers are added to intermediate layers to help with convergence. Glorot and Bengio [8] proposed to adopt a properly scaled uniform distribution for initialization. This is called “Xavier” initialization in [16]. Its derivation is based on the assumption that the activations are linear. This assumption is invalid for ReLU and PReLU.

In the following, we derive a theoretically more sound initialization by taking ReLU/PReLU into account. In our experiments, our initialization method allows for extremely deep models (*e.g.*, 30 conv/fc layers) to converge, while the “Xavier” method [8] cannot.

**Forward Propagation Case.** Our derivation mainly follows [8]. The central idea is to investigate the variance of the responses in each layer. For a conv layer, a response is:

$$\mathbf{y}_l = \mathbf{W}_l \mathbf{x}_l + \mathbf{b}_l. \quad (7)$$

Here,  $\mathbf{x}$  is a  $k^2 c$ -by-1 vector that represents co-located  $k \times k$  pixels in  $c$  input channels.  $k$  is the spatial filter-size of the layer. With  $n = k^2 c$  denoting the number of connections of a response,  $\mathbf{W}$  is a  $d$ -by- $n$  matrix, where  $d$  is the number of filters and each row of  $\mathbf{W}$  represents the weights of a filter.  $\mathbf{b}$  is a vector of biases, and  $\mathbf{y}$  is the response at a pixel of the output map. We use  $l$  to index a layer. We have  $\mathbf{x}_l = f(\mathbf{y}_{l-1})$  where  $f$  is the activation. We also have  $c_l = d_{l-1}$ .

We let the initialized elements in  $\mathbf{W}_l$  be independent and identically distributed (i.i.d.). As in [8], we assume that the elements in  $\mathbf{x}_l$  are also i.i.d., and  $\mathbf{x}_l$  and  $\mathbf{W}_l$  are independent of each other. Then we have:

$$\text{Var}[\mathbf{y}_l] = n_l \text{Var}[\mathbf{w}_l \mathbf{x}_l], \quad (8)$$

where now  $y_l$ ,  $x_l$ , and  $w_l$  represent the random variables of each element in  $\mathbf{y}_l$ ,  $\mathbf{W}_l$ , and  $\mathbf{x}_l$  respectively. We let  $w_l$  have zero mean. Then the variance of the product of independent variables gives us:

$$\text{Var}[\mathbf{y}_l] = n_l \text{Var}[\mathbf{w}_l] E[\mathbf{x}_l^2]. \quad (9)$$

Here  $E[\mathbf{x}_l^2]$  is the expectation of the square of  $x_l$ . It is worth noticing that  $E[\mathbf{x}_l^2] \neq \text{Var}[\mathbf{x}_l]$  unless  $x_l$  has zero mean. For ReLU,  $x_l = \max(0, y_{l-1})$  and thus it does not have zero mean. This will lead to a conclusion different from [8].

If we let  $w_{l-1}$  have a symmetric distribution around zero and  $b_{l-1} = 0$ , then  $y_{l-1}$  has zero mean and has a symmetric distribution around zero. This leads to  $E[\mathbf{x}_l^2] = \frac{1}{2} \text{Var}[\mathbf{y}_{l-1}]$  when  $f$  is ReLU. Putting this into Eqn.(9), we obtain:

$$\text{Var}[\mathbf{y}_l] = \frac{1}{2} n_l \text{Var}[\mathbf{w}_l] \text{Var}[\mathbf{y}_{l-1}]. \quad (10)$$

With  $L$  layers put together, we have:

$$\text{Var}[\mathbf{y}_L] = \text{Var}[\mathbf{y}_1] \left( \prod_{l=2}^L \frac{1}{2} n_l \text{Var}[\mathbf{w}_l] \right). \quad (11)$$

This product is the key to the initialization design. A proper initialization method should avoid reducing or magnifying the magnitudes of input signals exponentially. So we expect the above product to take a proper scalar (*e.g.*, 1). A sufficient condition is:

$$\frac{1}{2} n_l \text{Var}[\mathbf{w}_l] = 1, \quad \forall l. \quad (12)$$

This leads to a zero-mean Gaussian distribution whose standard deviation (std) is  $\sqrt{2/n_l}$ . This is our way of initialization. We also initialize  $\mathbf{b} = 0$ .

For the first layer ( $l = 1$ ), we should have  $n_1 \text{Var}[\mathbf{w}_1] = 1$  because there is no ReLU applied on the input signal. But the factor 1/2 does not matter if it just exists on one layer. So we also adopt Eqn.(12) in the first layer for simplicity.

**Backward Propagation Case.** For back-propagation, the gradient of a conv layer is computed by:

$$\Delta \mathbf{x}_l = \hat{\mathbf{W}}_l \Delta \mathbf{y}_l. \quad (13)$$

Here we use  $\Delta \mathbf{x}$  and  $\Delta \mathbf{y}$  to denote gradients ( $\frac{\partial \mathcal{E}}{\partial \mathbf{x}}$  and  $\frac{\partial \mathcal{E}}{\partial \mathbf{y}}$ ) for simplicity.  $\Delta \mathbf{y}$  represents  $k$ -by- $k$  pixels in  $d$  channels, and is reshaped into a  $k^2 d$ -by-1 vector. We denote  $\hat{n} = k^2 d$ . Note that  $\hat{n} \neq n = k^2 c$ .  $\hat{\mathbf{W}}$  is a  $c$ -by- $\hat{n}$  matrix where the filters are rearranged in the way of back-propagation. Note that  $\mathbf{W}$  and  $\hat{\mathbf{W}}$  can be reshaped from each other.  $\Delta \mathbf{x}$  is a  $c$ -by-1 vector representing the gradient at a pixel of this layer. As above, we assume that  $w_l$  and  $\Delta y_l$  are independent of each other, then  $\Delta x_l$  has zero mean for all  $l$ , when  $w_l$  is initialized by a symmetric distribution around zero.

In back-propagation we also have  $\Delta y_l = f'(y_l) \Delta x_{l+1}$  where  $f'$  is the derivative of  $f$ . For the ReLU case,  $f'(y_l)$  is zero or one with equal probabilities. We assume that  $f'(y_l)$  and  $\Delta x_{l+1}$  are independent of each other. Thus we have  $E[\Delta y_l] = E[\Delta x_{l+1}]/2 = 0$ , and also  $E[(\Delta y_l)^2] = \text{Var}[\Delta y_l] = \frac{1}{2} \text{Var}[\Delta x_{l+1}]$ . Then we compute the variance of the gradient in Eqn.(13):

$$\begin{aligned} \text{Var}[\Delta x_l] &= \hat{n}_l \text{Var}[\mathbf{w}_l] \text{Var}[\Delta \mathbf{y}_l] \\ &= \frac{1}{2} \hat{n}_l \text{Var}[\mathbf{w}_l] \text{Var}[\Delta x_{l+1}]. \end{aligned} \quad (14)$$

The scalar 1/2 in both Eqn.(14) and Eqn.(10) is the result of ReLU, though the derivations are different. With  $L$  layers put together, we have:

$$\text{Var}[\Delta x_2] = \text{Var}[\Delta x_{L+1}] \left( \prod_{l=2}^L \frac{1}{2} \hat{n}_l \text{Var}[\mathbf{w}_l] \right). \quad (15)$$

We consider a sufficient condition that the gradient is not exponentially large/small:

$$\frac{1}{2} \hat{n}_l \text{Var}[\mathbf{w}_l] = 1, \quad \forall l. \quad (16)$$



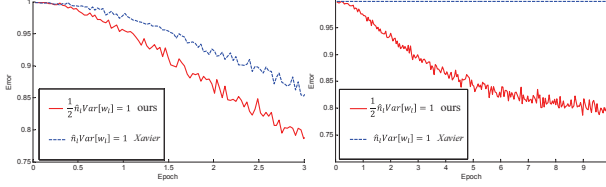


Figure 3. **Left:** convergence of a **22-layer** model (B in Table 3). The x-axis is training epochs. The y-axis is the top-1 val error. Both our initialization (red) and “Xavier” (blue) [8] lead to convergence, but ours starts reducing error earlier. **Right:** convergence of a **30-layer** model. Our initialization is able to make it converge, but “Xavier” completely stalls. We use ReLU in both figures.

The only difference between this equation and Eqn.(12) is that  $\hat{n}_l = k_l^2 d_l$  while  $n_l = k_l^2 c_l = k_l^2 d_{l-1}$ . Eqn.(16) results in a zero-mean Gaussian distribution whose std is  $\sqrt{2/\hat{n}_l}$ .

For the first layer ( $l = 1$ ), we need not compute  $\Delta x_1$  because it represents the image domain. But we can still adopt Eqn.(16) in the first layer, for the same reason as in the forward propagation case - the factor of a single layer does not make the overall product exponentially large/small.

We note that it is sufficient to use either Eqn.(16) or Eqn.(12) alone. For example, if we use Eqn.(16), then in Eqn.(15) the product  $\prod_{l=2}^L \frac{1}{2} \hat{n}_l \text{Var}[w_l] = 1$ , and in Eqn.(11) the product  $\prod_{l=2}^L \frac{1}{2} n_l \text{Var}[w_l] = \prod_{l=2}^L n_l / \hat{n}_l = c_2 / d_L$ , which is not a diminishing number in common network designs. This means that if the initialization properly scales the backward signal, then this is also the case for the forward signal; and vice versa. For all models in this paper, both forms can make them converge.

**Analysis.** If the forward/backward signal is inappropriately scaled by a factor  $\beta$  in each layer, then the final propagated signal will be rescaled by a factor of  $\beta^L$  after  $L$  layers, where  $L$  can represent some or all layers. When  $L$  is large, if  $\beta > 1$ , this leads to extremely amplified signals and an algorithm output of infinity; if  $\beta < 1$ , this leads to diminishing signals. In either case, the algorithm does not converge - it diverges in the former case, and stalls in the latter.

Our derivation also explains why the constant standard deviation of 0.01 makes some deeper networks stall [29]. We take “model B” in the VGG team’s paper [29] as an example. This model has 10 conv layers all with  $3 \times 3$  filters. The filter numbers ( $d_l$ ) are 64 for the 1st and 2nd layers, 128 for the 3rd and 4th layers, 256 for the 5th and 6th layers, and 512 for the rest. The std computed by Eqn.(16) ( $\sqrt{2/\hat{n}_l}$ ) is 0.059, 0.042, 0.029, and 0.021 when the filter numbers are 64, 128, 256, and 512 respectively. If the std is initialized as 0.01, the std of the gradient propagated from conv10 to conv2 is  $1/(5.9 \times 4.2^2 \times 2.9^2 \times 2.1^4) = 1/(1.7 \times 10^4)$  of what we derive. This number may explain why diminishing gradients were observed in experiments.

It is also worth noticing that the variance of the input

signal can be roughly preserved from the first layer to the last. In cases when the input signal is not normalized (e.g., in  $[-128, 128]$ ), its magnitude can be so large that the softmax operator will overflow. A solution is to normalize the input signal, but this may impact other hyper-parameters. Another solution is to include a small factor on the weights among all or some layers, e.g.,  $\sqrt[4]{1/128}$  on  $L$  layers. In practice, we use a std of 0.01 for the first two fc layers and 0.001 for the last. These numbers are smaller than they should be (e.g.,  $\sqrt{2/4096}$ ) and will address the normalization issue of images whose range is about  $[-128, 128]$ .

For the initialization in the PReLU case, it is easy to show that Eqn.(12) becomes:  $\frac{1}{2}(1 + a^2)n_l \text{Var}[w_l] = 1$ , where  $a$  is the initialized value of the coefficients. If  $a = 0$ , it becomes the ReLU case; if  $a = 1$ , it becomes the linear case (the same as [8]). Similarly, Eqn.(16) becomes  $\frac{1}{2}(1 + a^2)\hat{n}_l \text{Var}[w_l] = 1$ .

**Comparisons with “Xavier” Initialization [8].** The main difference between our derivation and the “Xavier” initialization [8] is that we address the rectifier nonlinearities<sup>3</sup>. The derivation in [8] only considers the linear case, and its result is given by  $n_l \text{Var}[w_l] = 1$  (the forward case), which can be implemented as a zero-mean Gaussian distribution whose std is  $\sqrt{1/n_l}$ . When there are  $L$  layers, the std will be  $1/\sqrt{2}^L$  of our derived std. This number, however, is not small enough to completely stall the convergence of the models actually used in our paper (Table 3, up to 22 layers) as shown by experiments. Figure 3(left) compares the convergence of a 22-layer model. Both methods are able to make them converge. But ours starts reducing error earlier. We also investigate the possible impact on accuracy. For the model in Table 2 (using ReLU), the “Xavier” initialization method leads to 33.90/13.44 top-1/top-5 error, and ours leads to 33.82/13.34. We have not observed clear superiority of one to the other on accuracy.

Next, we compare the two methods on extremely deep models with up to 30 layers (27 conv and 3 fc). We add up to sixteen conv layers with  $256 \ 2 \times 2$  filters in the model in Table 1. Figure 3(right) shows the convergence of the 30-layer model. Our initialization is able to make the extremely deep model converge. On the contrary, the “Xavier” method completely stalls the learning, and the gradients are diminishing as monitored in the experiments.

These studies demonstrate that we are ready to investigate extremely deep, rectified models by using a more principled initialization method. But in our current experiments on ImageNet, we have not observed the benefit from training extremely deep models. For example, the aforementioned 30-layer model has 38.56/16.59 top-1/top-5 error,

<sup>3</sup>There are other minor differences. In [8], the derived variance is adopted for uniform distributions, and the forward and backward cases are averaged. But it is straightforward to adopt their conclusion for Gaussian distributions and for the forward or backward case only.

input size	VGG-19 [29]	model A	model B	model C
224	3×3, 64 3×3, 64 2×2 pool, /2	7×7, 96, /2	7×7, 96, /2	7×7, 96, /2
112	3×3, 128 3×3, 128 2×2 pool, /2	2×2 pool, /2	2×2 pool, /2	2×2 pool, /2
56	3×3, 256 3×3, 256 3×3, 256 3×3, 256 2×2 pool, /2	3×3, 256 3×3, 256 3×3, 256 3×3, 256 2×2 pool, /2	3×3, 256 3×3, 256 3×3, 256 3×3, 256 2×2 pool, /2	3×3, 384 3×3, 384 3×3, 384 3×3, 384 2×2 pool, /2
28	3×3, 512 3×3, 512 3×3, 512 3×3, 512 2×2 pool, /2	3×3, 512 3×3, 512 3×3, 512 3×3, 512 2×2 pool, /2	3×3, 512 3×3, 512 3×3, 512 3×3, 512 2×2 pool, /2	3×3, 768 3×3, 768 3×3, 768 3×3, 768 2×2 pool, /2
14	3×3, 512 3×3, 512 3×3, 512 3×3, 512 2×2 pool, /2	3×3, 512 3×3, 512 3×3, 512 3×3, 512 spp	3×3, 512 3×3, 512 3×3, 512 3×3, 512 spp	3×3, 896 3×3, 896 3×3, 896 3×3, 896 spp
fc1, fc2, fc3		4096, 4096, 1000		
depth	19	19	22	22
comp.	1.96	1.90	2.32	5.30

Table 3. Architectures of large models. Here “/2” denotes a stride of 2. The “spp” layer [12] produces a 4-level {7, 3, 2, 1} pyramid. The complexity (comp.) is operations in  $10^{10}$ .

which is clearly worse than the error of the 14-layer model in Table 2 (33.82/13.34).

We found that this degradation is because of the increase of training error when the model is deeper. Such a degradation is still an open problem. Accuracy saturation or degradation due to depth was also observed in [29, 11, 38]. In [29], the 16-layer and 19-layer models perform comparably in image classification. In [11], aggressively increasing the depth leads to saturated or degraded accuracy. In the speech recognition research of [38], the deep models degrade when using more than 8 hidden layers (all being fc).

Though our attempts of extremely deep models have not shown benefits on accuracy, our initialization paves a foundation for further study on increasing depth. We hope this will be helpful in understanding deep networks.

### 2.3. Discussion on Rectifiers

The analysis in Sec. 2.1 and 2.2 involves the “rectified” units that are *asymmetric* activation functions, unlike many activations (e.g., tanh) that are symmetric. This leads to some fundamental differences. The conclusions involving Eqn.(6) (for FIM) and Eqn.(9) (for initialization) are heavily biased by the fact that  $E[f]$  is greater than zero in the case of ReLU. The asymmetric behavior requires algorithmic changes that take this effect into account. Our paper provides some explorations along this direction.

## 3. Architectures and Implementation

The above investigations provide guidelines of designing our architectures, introduced as follows.

Our baseline is the 19-layer model (A) in Table 3. For a better comparison, we also list the VGG-19 model [29]. Our model A has the following modifications on VGG-19: (i) in

the first layer, we use a filter size of  $7 \times 7$  and a stride of 2; (ii) we move the other three conv layers on the two largest feature maps (224, 112) to the smaller feature maps (56, 28, 14). The time complexity (Table 3, last row) is roughly unchanged because the deeper layers have more filters; (iii) we use spatial pyramid pooling (SPP) [12] before the first fc layer. The pyramid has 4 levels - the numbers of bins are  $7 \times 7$ ,  $3 \times 3$ ,  $2 \times 2$ , and  $1 \times 1$ , for a total of 63 bins.

It is worth noticing that we have no evidence that our model A is a better *architecture* than VGG-19, though our model A has better results than VGG-19’s result reported by [29]. In our earlier experiments with less scale augmentation, we observed that our model A and our reproduced VGG-19 (with SPP and our initialization) are comparable. The main purpose of using model A is for faster running speed. The actual running time of the conv layers on larger feature maps is slower than those on smaller feature maps, when their time complexity is the same. In our four-GPU implementation, our model A takes 2.6s per mini-batch (128), and our reproduced VGG-19 takes 3.0s, evaluated on four Nvidia K20 GPUs.

In Table 3, our model B is a deeper version of A. It has three extra conv layers. Our model C is a wider (with more filters) version of B. The width substantially increases the complexity, and its time complexity is about  $2.3 \times$  of B (Table 3, last row). Training A/B on four K20 GPUs, or training C on eight K40 GPUs, takes about 3-4 weeks.

We choose to increase the model width instead of depth, because deeper models have only diminishing improvement or even degradation on accuracy. As we will show, the deeper model B is just marginally better than A.

While all models in Table 3 are very large, we have not observed severe overfitting. We attribute this to the aggressive data augmentation used throughout the whole training procedure, as introduced below.

**Training.** Our training mostly follows [18, 14, 2, 12, 29]. From a resized image whose shorter side is  $s$ , a  $224 \times 224$  crop is randomly sampled, with the per-pixel mean subtracted. The scale  $s$  is randomly jittered in the range of [256, 512], following [29]. A sample is horizontally flipped at a chance of 50%. Random color altering [18] is also used.

Unlike [29] that applies scale jittering only during fine-tuning, we apply it at the beginning. Unlike [29] that initializes a deeper model using a shallower one, we directly train the very deep model using our initialization described in Sec. 2.2 (Eqn.(16)). Our end-to-end training may help improve accuracy, as it may avoid poorer local optima.

Other hyper-parameters that might be important are as follows. The weight decay is 0.0005, and momentum is 0.9. Dropout (50%) is used in the first two fc layers. The mini-batch size is fixed as 128. The learning rate is  $1e-2$ ,  $1e-3$ , and  $1e-4$ , and is switched when the error plateaus. The total number of epochs is about 80 for each model.

model A	ReLU		PReLU	
scale $s$	top-1	top-5	top-1	top-5
256	26.25	8.25	<b>25.81</b>	<b>8.08</b>
384	24.77	7.26	<b>24.20</b>	<b>7.03</b>
480	25.46	7.63	<b>24.83</b>	<b>7.39</b>
multi-scale	24.02	6.51	<b>22.97</b>	<b>6.28</b>

Table 4. Comparisons between ReLU/PReLU on model A in ImageNet 2012 using dense testing.

**Testing.** We adopt the strategy of “multi-view testing on feature maps” used in the SPP-net paper [12]. We further improve this strategy using the dense sliding window method in [28, 29]. We first apply the convolutional layers on the resized full image and obtain the last convolutional feature map. In the feature map, each  $14 \times 14$  window is pooled using the SPP layer [12]. The fc layers are then applied on the pooled features to compute the scores. This is also done on the horizontally flipped images. The scores of all dense sliding windows are averaged [28, 29]. We further average the scores at multiple scales as in [12].

**Multi-GPU Implementation.** We adopt a simple variant of Krizhevsky’s method [17] for parallel training on multiple GPUs. We adopt “data parallelism” [17] on the conv layers. The GPUs are synchronized before the first fc layer. Then the forward/backward propagations of the fc layers are performed on a single GPU - this means that we do not parallelize the computation of the fc layers. The time cost of the fc layers is low, so it is not necessary to parallelize them. This leads to a simpler implementation than the “model parallelism” in [17]. We implement based on our modification of the Caffe library [16]. We do not increase the mini-batch size (128) because the accuracy may be decreased [17].

## 4. Experiments on ImageNet

We perform the experiments on the 1000-class ImageNet 2012 dataset [26] which contains about 1.2 million training images, 50,000 validation images, and 100,000 test images (with no published labels). The results are measured by top-1/top-5 error rates [26]. We only use the provided data for training. All results are evaluated on the validation set, except for the final test results in Table 7.

**Comparisons between ReLU and PReLU.** In Table 4, we compare ReLU and PReLU on the large model A. We use the channel-wise version of PReLU. For fair comparisons, both ReLU/PReLU models are trained using the same total number of epochs, and the learning rates are also switched after running the same number of epochs. Figure 4 shows the train/val error during training. PReLU converges faster than ReLU. Moreover, PReLU has lower train error *and* val error than ReLU *throughout* the training procedure.

Table 4 shows the results at three scales and the multi-scale combination. For the multi-scale combination,

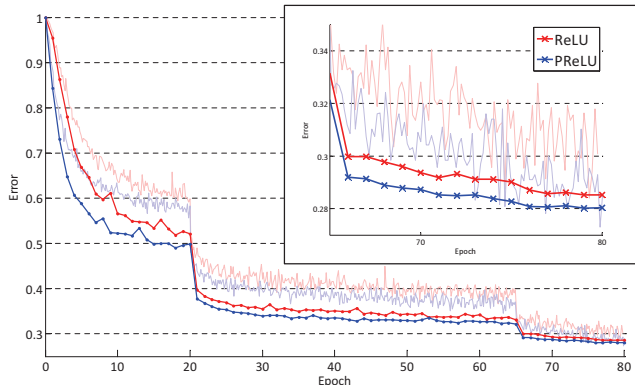


Figure 4. Convergence of ReLU (red) vs. PReLU (blue) of model A on ImageNet. Light lines denote the training error of the current mini-batch, and dark lines denote validation error of the center crops. In the zoom-in is the last few epochs. Learning rates are switched at 20 and 65 epochs.

PReLU reduces the top-1 error by 1.05% and the top-5 error by 0.23% compared with ReLU. The results in Table 2 and Table 4 consistently show that PReLU improves both small and large models. This improvement is with almost no computational cost.

**Comparisons of Single-model Results.** Next we compare single-model results. We first show 10-view testing results [18] in Table 5. Here, each view is a 224-crop. The 10-view results of VGG-16 are based on our testing using the publicly released model [29] as it is not reported in [29]. Our best 10-view result is 7.38% (Table 5). Our other models also outperform the existing results.

Table 6 shows the comparisons of single-model results, which are all obtained using multi-scale and multi-view (or dense) test. For our models, the combination weights for all scales are equal. Our baseline model (A+ReLU, 6.51%) is already substantially better than the single-model result of 7.1% reported for VGG-19 in the latest update of [29] (arXiv v5). We believe that this gain is mainly due to our end-to-end training, without the need of pre-training shallow models.

Moreover, our best single model (C, PReLU) has **5.71%** top-5 error. This result is better than all multi-model results in ILSVRC 14 (Table 7). Comparing A+PReLU with B+PReLU, we see that the 19-layer model and the 22-layer model perform comparably. On the other hand, increasing the width (C vs. B, Table 6) can still improve accuracy. This indicates that when the models are deep enough, the width becomes an essential factor for accuracy.

**Comparisons of Multi-model Results.** We combine six models including those in Table 6. For the time being we have trained only one model with architecture C. The other models have accuracy inferior to C by considerable mar-



model	top-1	top-5
SPP [12]	29.68	10.95
VGG-16 [29]	28.07 <sup>†</sup>	9.33 <sup>†</sup>
GoogLeNet [33]	-	9.15
A, ReLU	26.48	8.59
A, PReLU	25.59	8.23
B, PReLU	25.53	8.13
C, PReLU	<b>24.27</b>	<b>7.38</b>

Table 5. Single-model **10-view** results for ImageNet 2012 val set. <sup>†</sup>: Based on our tests.

	method	top-1	top-5
in ILSVRC 14	SPP [12]	27.86	9.08 <sup>†</sup>
	VGG [29]	-	8.43 <sup>†</sup>
	GoogLeNet [33]	-	7.89
post ILSVRC 14	VGG [29] (arXiv v2)	24.8	7.5
	VGG [29] (arXiv v5)	24.4	7.1
	ours (A, ReLU)	24.02	6.51
	ours (A, PReLU)	22.97	6.28
	ours (B, PReLU)	22.85	6.27
	ours (C, PReLU)	<b>21.59</b>	<b>5.71</b>

Table 6. **Single-model** results for ImageNet 2012 val set. <sup>†</sup>: Evaluated from the test set.

	method	top-5 (test)
in ILSVRC 14	SPP [12]	8.06
	VGG [29]	7.32
	GoogLeNet [33]	6.66
post ILSVRC 14	VGG [29] (arXiv v5)	6.8
	<b>ours</b>	<b>4.94</b>

Table 7. **Multi-model** results for the ImageNet 2012 test set.

gins. The multi-model results are in Table 7. Our result is **4.94%** top-5 error on the test set. Our result is 1.7% better than the ILSVRC 2014 winner (GoogLeNet, 6.66% [33]), which represents a 26% relative improvement.<sup>4</sup>

**Comparisons with Human Performance from [26].** Rusakovsky *et al.* [26] recently reported that human performance yields a 5.1% top-5 error on the ImageNet dataset. Our result (4.94%) exceeds the reported human-level performance. The investigation in [26] suggests that algorithms can do a better job on fine-grained recognition (*e.g.*, 120 species of dogs in the dataset). The second row of Figure 5 shows some example fine-grained objects successfully recognized by our method - “coucal”, “komondor”, and “yellow lady’s slipper”. While humans can easily recognize these objects as a bird, a dog, and a flower, it is non-trivial for most humans to tell their species. On the negative side, our algorithm still makes mistakes in cases that are not difficult for humans, especially for those requiring context

<sup>4</sup>Concurrently, a Batch Normalization method [15] achieves results on par with ours: 5.82% error for a single model (*vs.* ours 5.71%), and 4.82% error for an ensemble (*vs.* ours 4.94%).



Figure 5. Example validation images successfully classified by our method. For each image, the ground-truth label and the top-5 labels predicted by our method are listed.

understanding or high-level knowledge.

While our algorithm produces a superior result on this particular dataset, this does not indicate that machine vision outperforms human vision on object recognition in general. On recognizing elementary object categories (*i.e.*, common objects or concepts in daily lives) such as the Pascal VOC task [5], machines still have obvious errors in cases that are trivial for humans. Nevertheless, we believe that our results show the tremendous potential of machine algorithms to match human-level performance on visual recognition.

**Object Detection on PASCAL VOC.** An important application of ImageNet-trained models is for transfer learning [7] on other recognition tasks. We evaluate these models on PASCAL VOC 2007 object detection [5]. We use the recent *Fast R-CNN* [6] implementation (with public code). With an ImageNet-trained model, we fine-tune the detectors on VOC 2007 *trainval* and evaluate on the test set. The detection results are in Table 8, which are consistent with ImageNet classification results. Note that using the same model A, PReLU (68.4%) improves over ReLU (67.6%) on this transfer learning task, suggesting that better features have been learned with the help of PReLU.

network	VGG-16	A+ReLU	A+PReLU	C+PReLU
mAP(%)	66.9 [6]	67.6	68.4	<b>69.2</b>

Table 8. **Object detection** mAP on PASCAL VOC 2007 using Fast R-CNN [6] on different pre-trained nets.

## References

- [1] F. Agostinelli, M. Hoffman, P. Sadowski, and P. Baldi. Learning activation functions to improve deep neural networks. *arXiv:1412.6830*, 2014.



- [2] K. Chatfield, K. Simonyan, A. Vedaldi, and A. Zisserman. Return of the devil in the details: Delving deep into convolutional nets. In *BMVC*, 2014.
- [3] D. Ciresan, U. Meier, and J. Schmidhuber. Multi-column deep neural networks for image classification. In *CVPR*, 2012.
- [4] J. Deng, W. Dong, R. Socher, L.-J. Li, K. Li, and L. Fei-Fei. Imagenet: A large-scale hierarchical image database. In *CVPR*, 2009.
- [5] M. Everingham, L. Van Gool, C. K. Williams, J. Winn, and A. Zisserman. The Pascal Visual Object Classes (VOC) Challenge. *IJCV*, pages 303–338, 2010.
- [6] R. Girshick. Fast R-CNN. *arXiv:1504.08083*, 2015.
- [7] R. Girshick, J. Donahue, T. Darrell, and J. Malik. Rich feature hierarchies for accurate object detection and semantic segmentation. In *CVPR*, 2014.
- [8] X. Glorot and Y. Bengio. Understanding the difficulty of training deep feedforward neural networks. In *International Conference on Artificial Intelligence and Statistics*, 2010.
- [9] X. Glorot, A. Bordes, and Y. Bengio. Deep sparse rectifier networks. In *Proceedings of the 14th International Conference on Artificial Intelligence and Statistics*, pages 315–323, 2011.
- [10] I. J. Goodfellow, D. Warde-Farley, M. Mirza, A. Courville, and Y. Bengio. Maxout networks. *arXiv:1302.4389*, 2013.
- [11] K. He and J. Sun. Convolutional neural networks at constrained time cost. *arXiv:1412.1710*, 2014.
- [12] K. He, X. Zhang, S. Ren, and J. Sun. Spatial pyramid pooling in deep convolutional networks for visual recognition. *arXiv:1406.4729v2*, 2014.
- [13] G. E. Hinton, N. Srivastava, A. Krizhevsky, I. Sutskever, and R. R. Salakhutdinov. Improving neural networks by preventing co-adaptation of feature detectors. *arXiv:1207.0580*, 2012.
- [14] A. G. Howard. Some improvements on deep convolutional neural network based image classification. *arXiv:1312.5402*, 2013.
- [15] S. Ioffe and C. Szegedy. Batch normalization: Accelerating deep network training by reducing internal covariate shift. *arXiv:1502.03167*, 2015.
- [16] Y. Jia, E. Shelhamer, J. Donahue, S. Karayev, J. Long, R. Girshick, S. Guadarrama, and T. Darrell. Caffe: Convolutional architecture for fast feature embedding. *arXiv:1408.5093*, 2014.
- [17] A. Krizhevsky. One weird trick for parallelizing convolutional neural networks. *arXiv:1404.5997*, 2014.
- [18] A. Krizhevsky, I. Sutskever, and G. Hinton. Imagenet classification with deep convolutional neural networks. In *NIPS*, 2012.
- [19] Y. LeCun, B. Boser, J. S. Denker, D. Henderson, R. E. Howard, W. Hubbard, and L. D. Jackel. Backpropagation applied to handwritten zip code recognition. *Neural computation*, 1989.
- [20] Y. LeCun, L. Bottou, G. B. Orr, and K.-R. Müller. Efficient backprop. In *Neural Networks: Tricks of the Trade*, pages 9–50. Springer, 1998.
- [21] C.-Y. Lee, S. Xie, P. Gallagher, Z. Zhang, and Z. Tu. Deeply-supervised nets. *arXiv:1409.5185*, 2014.
- [22] M. Lin, Q. Chen, and S. Yan. Network in network. *arXiv:1312.4400*, 2013.
- [23] A. L. Maas, A. Y. Hannun, and A. Y. Ng. Rectifier nonlinearities improve neural network acoustic models. In *ICML*, 2013.
- [24] V. Nair and G. E. Hinton. Rectified linear units improve restricted boltzmann machines. In *ICML*, pages 807–814, 2010.
- [25] T. Raiko, H. Valpola, and Y. LeCun. Deep learning made easier by linear transformations in perceptrons. In *International Conference on Artificial Intelligence and Statistics*, 2012.
- [26] O. Russakovsky, J. Deng, H. Su, J. Krause, S. Satheesh, S. Ma, Z. Huang, A. Karpathy, A. Khosla, M. Bernstein, et al. Imagenet large scale visual recognition challenge. *arXiv:1409.0575*, 2014.
- [27] A. M. Saxe, J. L. McClelland, and S. Ganguli. Exact solutions to the nonlinear dynamics of learning in deep linear neural networks. *arXiv:1312.6120*, 2013.
- [28] P. Sermanet, D. Eigen, X. Zhang, M. Mathieu, R. Fergus, and Y. LeCun. Overfeat: Integrated recognition, localization and detection using convolutional networks. 2014.
- [29] K. Simonyan and A. Zisserman. Very deep convolutional networks for large-scale image recognition. *arXiv:1409.1556*, 2014.
- [30] N. Srivastava, G. Hinton, A. Krizhevsky, I. Sutskever, and R. Salakhutdinov. Dropout: A simple way to prevent neural networks from overfitting. *The Journal of Machine Learning Research*, pages 1929–1958, 2014.
- [31] R. K. Srivastava, J. Masci, S. Kazerounian, F. Gomez, and J. Schmidhuber. Compete to compute. In *NIPS*, pages 2310–2318, 2013.
- [32] Y. Sun, Y. Chen, X. Wang, and X. Tang. Deep learning face representation by joint identification-verification. In *NIPS*, 2014.
- [33] C. Szegedy, W. Liu, Y. Jia, P. Sermanet, S. Reed, D. Anguelov, D. Erhan, V. Vanhoucke, and A. Rabinovich. Going deeper with convolutions. *arXiv:1409.4842*, 2014.
- [34] Y. Taigman, M. Yang, M. Ranzato, and L. Wolf. Deepface: Closing the gap to human-level performance in face verification. In *CVPR*, 2014.
- [35] T. Vatanen, T. Raiko, H. Valpola, and Y. LeCun. Pushing stochastic gradient towards second-order methods—backpropagation learning with transformations in nonlinearities. In *Neural Information Processing*, pages 442–449. Springer, 2013.
- [36] L. Wan, M. Zeiler, S. Zhang, Y. L. Cun, and R. Fergus. Regularization of neural networks using dropconnect. In *ICML*, pages 1058–1066, 2013.
- [37] M. D. Zeiler and R. Fergus. Visualizing and understanding convolutional neural networks. In *ECCV*, 2014.
- [38] M. D. Zeiler, M. Ranzato, R. Monga, M. Mao, K. Yang, Q. V. Le, P. Nguyen, A. Senior, V. Vanhoucke, J. Dean, and G. E. Hinton. On rectified linear units for speech processing. In *ICASSP*, 2013.